Influence of metal ions intercalation on the vibrational dynamics of water confined between MXene layers

Naresh C. Osti,[1,*] Michael Naguib,[2] Karthik Ganeshan,[3] Yun K. Shin,[3] Alireza Ostadhossein,[4] Adri C. T. van Duin,[3] Yongqiang Cheng,[1] Luke L. Daemen,[1] Yury Gogotsi,[5] Eugene Mamontov,[1] and Alexander I. Kolesnikov[1,†]

[1]*Neutron Scattering Division, Oak Ridge National Laboratory, Oak Ridge, Tennessee 37831, USA*

[2]*Materials Science and Technology Division, Oak Ridge National Laboratory, Oak Ridge, Tennessee 37831, USA*

[3]*Department of Mechanical and Nuclear Engineering, Pennsylvania State University, University Park, Pennsylvania 16802, USA*

[4]*Department of Engineering Science and Mechanics, Pennsylvania State University, University Park, Pennsylvania 16802, USA*

[5]*Department of Materials Science and Engineering, and A. J. Drexel Nanomaterials Institute, Drexel University, Philadelphia, Pennsylvania 19104, USA*

(Received 28 July 2017; revised manuscript received 25 October 2017; published 21 November 2017)

Two-dimensional (2D) carbides and nitrides of early transition metals (MXenes) combine high conductivity with hydrophilic surfaces, which make them promising for energy storage, electrocatalysis, and water desalination. The effects of intercalated metal ions on the vibrational states of water confined in $Ti_3C_2T_x$ MXenes have been explored using inelastic neutron scattering (INS) and molecular-dynamics simulations to better understand the mechanisms that control MXenes' behavior in aqueous electrolytes, water purification, and other important applications. We observe an INS signal from water in all samples, pristine and with lithium, sodium, or potassium ions intercalated between the 2D $Ti_3C_2T_x$ layers. However, only a small amount of water is found to reside in $Ti_3C_2T_x$ intercalated with metal ions. Water in pristine $Ti_3C_2T_x$ is more disordered, with bulklike characteristics, in contrast to intercalated $Ti_3C_2T_x$, where water is more ordered, irrespective of the metal ions used for intercalation. The ordering of the confined water increases with the ion size. This finding is further confirmed from molecular-dynamics simulation, which showed an increase in interference of water molecules with increasing ion size resulting in a concomitant decrease in water mobility, therefore providing guidance to tailor MXene properties for energy and environmental applications.

DOI: 10.1103/PhysRevMaterials.1.065406

I. INTRODUCTION

MXenes [1,2] are two-dimensional (2D) transition metal carbides and nitrides, usually synthesized by selective etching of the "*A*" layers of MAX phases, where *A* is mostly aluminum, *M* is an early transition metal, and *X* is carbon and /or nitrogen, and they consist of $M_{n+1}X_n$ layers, where $n = 1, 2$, or 3. More than 20 different MXenes reported to date (Ti_2C, Ti_3C_2, Nb_4C_3, and others) have attracted much attention due to their 2D layered morphology and intriguing properties, such as conductivity and hydrophilicity, which make them promising materials for electrochemical applications [3–8]. In addition, the occurrence of oxygen, hydroxyl, and fluorine groups on MXene surfaces (defined by adding T to their chemical formula, e.g., $Ti_3C_2T_x$) allows their properties to be tuned. The calculated low work function of OH-terminated MXenes has illustrated the promise of these materials in power-efficient electronics [9]. Furthermore, because of the layered structure combined with hydrophilic groups on the surface, MXenes can hold water molecules between the layers, and they can also be intercalated by ions and molecules. It was found that the intercalation of guest molecules such as hydrazine [10,11] and K^+ ions [8] increases the *c*-lattice (*c*-*L*) parameter of $Ti_3C_2T_x$ MXene with a concomitant decrease in the amount of intercalated water between the MXene layers, controlling the electrochemical characteristics of these materials when used as batteries and supercapacitors. An increase in the interlayer spacing and an enhancement in the electrochemical performance of MXenes after intercalation have been reported [8,11,12]. However, it has not been well understood how the structure and dynamics of water confined between the MXene layers change after metal ions intercalation.

Confinement of water in matrices such as clays [13], carbon nanopores [14], and carbon nanotubes [15] results in its different structural and dynamical behavior compared to the bulk water phase. Since the $Ti_3C_2T_x$ surface is hydrophilic, it behaves similar to most of the clay materials [16]. Therefore, it is important to understand the vibrational dynamics of water molecules in order to shed light on the behavior of confined water in pristine and metal ions intercalated form of these 2D materials for their technical applications. Highly reduced translational diffusion of water after K^+ intercalation was observed from quasielastic neutron scattering (QENS) and molecular-dynamics simulation study [17]. This reduction in mobility is associated with the partial removal of water and the bonding of the remaining water molecules with the surface-terminating groups and intercalants. Inelastic neutron scattering (INS) is a powerful tool to resolve the bonding between the surfaces and the hydrogen bearing molecules (hydrogen and water) in confinement [18–21]. Previous INS study [22] showed changes in the vibrational states of MXene due to the deintercalation of water molecules confined between MXene layers. Further, removal of intercalated water molecules influences the covalency that exists in MXenes sheets and thereby impacts the vibrational dynamics of MXenes [23]. Here, using inelastic neutron scattering and molecular-dynamics simulations, we investigate the vibrational dynamics of water confined in pristine and metal ions intercalated $Ti_3C_2T_x$ MXenes.

*ostinc@ornl.gov

†kolesnikovai@ornl.gov

II. EXPERIMENT

A. Sample preparation

Ti_3AlC_2 powder with particle size $\leqslant 45\,\mu$m (more details about the synthesis of Ti_3AlC_2 can be found in Ref. [1]) was mixed with 48% HF aqueous solution and stirred for 24 h at ambient conditions. The solution was washed with deionized water until the pH of the solution reached higher than 4. The resulting $Ti_3C_2T_x$ (T_x = surface groups) powder was mixed with aqueous solutions of 2*M* LiOH, 2*M* NaOH, and 2*M* KOH separately, in a ratio of 1 g of $Ti_3C_2T_x$ to 10 mL, to obtain metal ion intercalated MXene. The resulting solutions were centrifuged after stirring for an hour to separate powders from the solutions. The settled MXenes powder was again mixed with freshly prepared 2*M* LiOH, 2*M* NaOH, and 2*M* KOH solutions individually with a ratio of 1 g of $Ti_3C_2T_x$ to 10 mL. Final centrifuging and decantation followed by filtration were performed to obtain pristine ($Ti_3C_2T_x$) and metal ions intercalated MXenes ($Ti_3C_2T_x$-K, $Ti_3C_2T_x$-Na, and $Ti_3C_2T_x$-Li) powders. The powders were kept at room temperature for 18 h for air drying. The x-ray diffraction (XRD) of air-dried MXenes was measured. The MXene samples were then annealed at 110 °C in vacuum for 4 h to remove bulk water. XRD of all the samples was collected after annealing to 110 °C. The $Ti_3C_2T_x$ sample was annealed at vacuum to 150 °C for 4 h to remove the trapped molecular hydrogen.

B. Neutron scattering

The Fine Resolution Fermi Chopper Spectrometer (SEQUOIA) [24,25] at the Spallation Neutron Source at Oak Ridge National Laboratory was used to measure the INS spectra of the water confined in pristine and metal ions intercalated MXenes. The spectra were collected using four incident neutron energies (E_i = 50, 160, 250, and 600 meV). INS spectra of pure water and 2*M* metal hydroxide solutions ($\sim$ 5 g) of Li, Na, and K were measured using the inverse geometry time-of-flight spectrometer VISION [26] at the same facility. All samples were placed into aluminum containers, and the INS spectra were collected at 7 K.

C. Molecular-dynamics simulation

All the MD simulations were performed in ReaxFF [27,28] within ADF (distributed by SCM; see http://www.scm.com). In our simulations, we had 320 Ti-surface atoms and 320 -OH groups. The model of the system, comprised of 1776 atoms (72 cations, 88 water molecules, and two layers of MXene), was first subjected to 200 steps of energy minimization followed by *NPT* at 300 K for 20 ps. A temperature damping constant of 100 fs and a pressure damping of 1000 fs were used, and the *a* and *b* lattice parameters were fixed for all the systems. The resulting system was subjected to an *NVT* simulation under a Berendsen thermostat with a temperature damping constant of 100 fs for 12.5 ps, followed by a production *NVT* simulation with a weak coupling of the thermostat (a temperature damping constant of 1000 fs) for 200 ps for data collection.

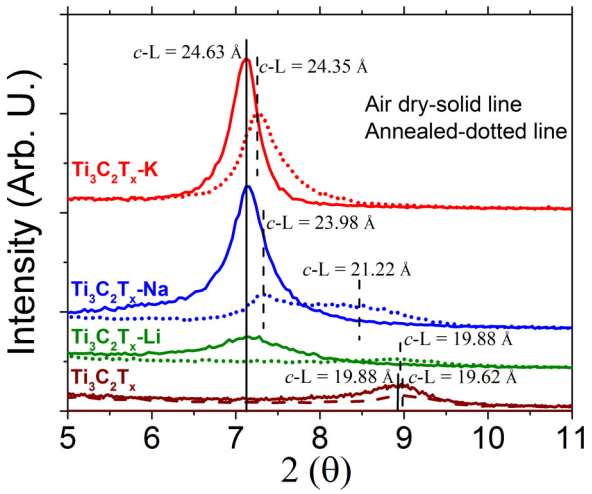

FIG. 1. XRD pattern of pristine and metal ions (Li^+, Na^+, and K^+) intercalated MXene before (solid lines) and after (dotted lines) vacuum annealing at 110 °C as specified in the figure along with corresponding peak positions and calculated *c*-*L* parameter values. Data for pristine and K^+-intercalated MXenes have been adapted from Ref. [17].

III. RESULTS AND DISCUSSION

X-ray diffraction (XRD) patterns of pristine and metal ions (Li^+, Na^+, and K^+) intercalated $Ti_3C_2T_x$ in two forms, air-dried at room temperature and vacuum-annealed at 110 °C, are presented in Fig. 1. A prominent peak, corresponding to the *c*-lattice (*c*-*L*) parameter of 19.88 Å, was observed for air-dried pristine $Ti_3C_2T_x$. Upon intercalation, the position of that peak shifts to a lower angle, indicating an increase in the *c*-*L* parameter, and suggesting the presence of some water molecules along with the metal ions between the MXene layers. There is a very small change in the *c*-*L* parameter of pristine $Ti_3C_2T_x$ after vacuum annealing, whereas metal ions intercalated samples show different behavior. Vacuum annealed K^+-intercalated $Ti_3C_2T_x$ ($Ti_3C_2T_x$-K) shows a very small reduction in the *c*-*L* parameter. Vacuum annealed Na^+-intercalated $Ti_3C_2T_x$ ($Ti_3C_2T_x$-Na) shows two peaks, one narrow and one broad, with the corresponding *c*-*L* parameters of 23.98 and 21.22 Å, respectively. In vacuum annealed Li^+-intercalated $Ti_3C_2T_x$ ($Ti_3C_2T_x$-Li), the value of the *c*-*L* parameter changes from 24.63 to 19.88 Å. The structural changes in Li^+- and Na^+-intercalated MXenes after annealing are not quite understood and might warrant a dedicated *in situ* time-resolved XRD study.

We studied the vibrational dynamics of water confined in vacuum annealed (110 °C) pristine and metal ions (Li^+, Na^+, and K^+) intercalated $Ti_3C_2T_x$ by using the INS technique. The INS spectra from hydrogen-containing materials predominantly represent the scattering on hydrogen atoms due to an anomalously large incoherent neutron-scattering cross section of hydrogen. Therefore, in our experiment, we measured various vibration modes of water molecules and hydroxyl groups (if present). Irrespective of the incident neutron energy, we observed (Fig. 2) that the intensity from pristine $Ti_3C_2T_x$ is about 2.8 times higher compared to ions intercalated $Ti_3C_2T_x$, which shows that intercalation removes a substantial amount

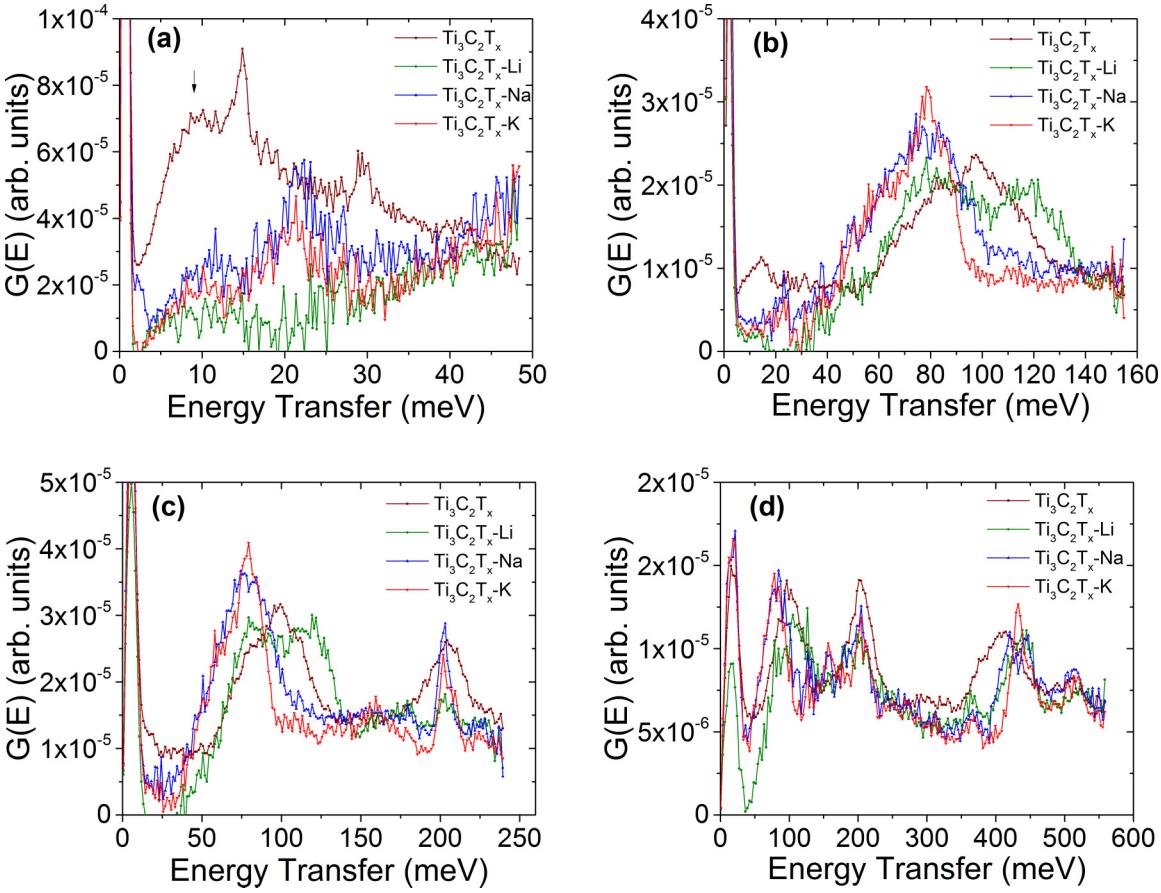

FIG. 2. GVDS of pristine and metal ions (Li^+, Na^+, and K^+) intercalated MXene measured at SEQUOIA with (a) $E_i = 50$ meV, (b) $E_i = 160$ meV, (c) $E_i = 250$ meV, and (d) $E_i = 600$ meV at $T = 7$ K. The intensity from pristine MXene has been divided by 2.8 for comparison purposes. The spectra shown in (a) for pristine MXene and for MXene intercalated with K^+ were adapted from Ref. [38], and the spectra for pristine MXene in (c) and (d) were reported earlier in [11].

of water that was present in pristine $Ti_3C_2T_x$. Our recent QENS study of water dynamics in $Ti_3C_2T_x$ and $Ti_3C_2T_x$-K has shown that water in the pristine $Ti_3C_2T_x$ is present in the gaps between stacks (a stack comprises a number of MXene layers, and a layer consists of a formula unit of MXene, i.e., two carbon atoms sandwiched between three titanium atoms), and there is no intercalated water between the layers [17]. Diffusivity of the interstack water was found to exhibit half of the bulk water value. K^+ intercalation allows water to stay between the $Ti_3C_2T_x$ layers, together with the metal ions, where water mobility decreases dramatically. In general, a larger amount of water in confinement is associated with higher diffusivity [29]. Water molecules in MXenes are expected to exhibit vibrational bands related to intermolecular translational (0–40 meV) and librational (40–140 meV) modes, as well as intramolecular H-O-H bending (∼205 meV) and O-H stretching (400−450 meV) modes, similar to water in clays [30], graphene oxide [31], zeolites [32], silicate sheets [33], and rutile nanoparticles [21]. The measured INS spectra were transformed to generalized vibrational density of states, GVDS, or $G(E)$ as follows:

$$G(E) = S(Q,E)\frac{E}{Q^2[n(E,T)+1]}, \quad (1)$$

where $S(Q, E)$ is a dynamical structure factor, E and Q are the energy and momentum transfer of neutrons, and $n(E,T) = [\exp(E/k_BT) - 1]^{-1}$ is a Bose population factor. Figure 2(a) shows the $G(E)$ spectra at low-energy transfer (measured with $E_i = 50$ meV), where the translational vibrational modes of water molecules are observed. There is an increase of intensity with a maximum around 8–10 meV for $Ti_3C_2T_x$ (indicated by an arrow in the figure). This peak maximum is close to the peak in the INS spectra of bulk amorphous water, ice-Ih, and other ice phases (around 6–10 meV), where it is related to the acoustic transverse modes in a hydrogen-bonded network of water molecules [34,35]. A similar peak in the spectra of Na^+- and K^+-intercalated samples is present, but strongly suppressed, while a broad peak around 20 meV is now observed. This peak corresponds to in-plane vibrations of Ti and C atoms (∼20 meV) in a simulated vibrational spectrum for a monolayer of $Ti_3C_2T_x$ [36]. Therefore, we can assign this peak in our spectra to the riding modes of water, which is totally confined in $Ti_3C_2T_x$. Hence, these spectra suggest the presence of only a minute amount of bulk water and hydrogen bonding between the water molecules and the $Ti_3C_2T_x$ surface [11]. In the GVDS spectrum of $Ti_3C_2T_x$-Li, there is a strong reduction in intensity at an energy transfer ∼20 meV, which is probably due to the very large neutron absorption cross section by Li atoms [37]. Two peaks in the

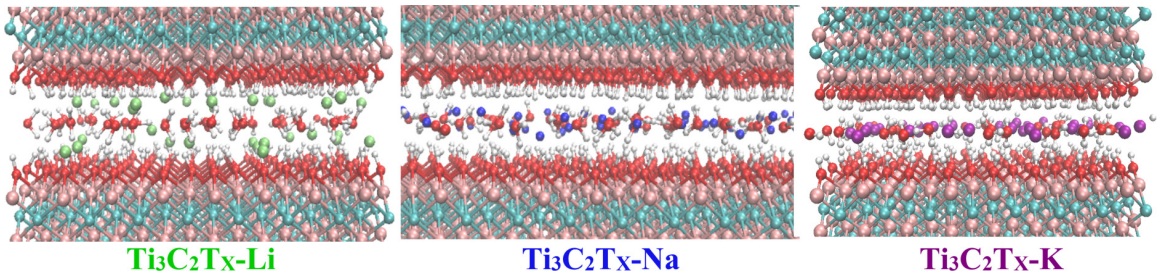

FIG. 3. Snapshots from the ReaxFF molecular-dynamics simulations at 300 K of the Li^+, Na^+, and K^+ intercalated $Ti_3C_2T_x$ layer. White, red, pink, and cyan atoms in the MXene layer represent H, O, Ti, and C, respectively. Green, blue, and purple atoms represent Li^+, Na^+, and K^+ ions, respectively.

pristine $Ti_3C_2T_x$ spectrum, at 14.7 and 29.4 meV, are attributed to the presence of trapped molecular hydrogen (H_2), which shows para $\leftrightarrow$ ortho transitions ($J = 0$ to 1 and $J = 1$ to 2 transitions, respectively) [38,39].

The effect of metal ions intercalation on the librational modes of water (energy range 50–140 meV) is presented in Fig. 2(b). The librational modes of the water molecule are influenced by the interaction with the confining surface, ions, and other nearby water molecules [32,40]. For a proton ordered ice (e.g., ice-VIII), the librational band shows three peaks due to libration of the water molecules around three orthogonal axes, but for proton disordered ice (e.g., ice-Ih) it appears as one broadband due to disorder in a hydrogen-bonded network of water molecules [35]. The presence of -OH groups gives a more separated peak, often around 120 meV. $Ti_3C_2T_x$ shows a broad peak (from 50 to 130 meV), indicating the presence of bulklike disordered confined water. After Na^+ and K^+ metal ions intercalation, there is a significant shift of the librational band to the left, indicating softening of the hydrogen bonds of the water molecules. Furthermore, the spectra become progressively narrower with an increase in the size of the intercalating metal ions, thus revealing a stronger effect for the bigger ions, such as K^+. However, the spectrum from $Ti_3C_2T_x$-Li is similar to that of bulklike water present in the $Ti_3C_2T_x$, with a negligible softening of the H bond compared to Na^+ and K^+ ions. In addition, it shows a prominent peak at $\sim$120 meV, indicating that the Li^+-intercalated $Ti_3C_2T_x$ contains more OH groups and fewer water molecules compared to Na^+ and K^+ ions intercalated samples.

The OH groups in $Ti_3C_2T_x$-Li should not contribute to the energy range of the water intramolecular bending mode around 200 meV, which is prominently demonstrated by Fig. 2(c). The GVDS spectra from all $Ti_3C_2T_x$ samples (pristine and metal ions intercalated) show a peak at $\sim$200 meV due to the intramolecular H-O-H bending mode, and this peak is the smallest for $Ti_3C_2T_x$-Li. The peak from $Ti_3C_2T_x$ is broader compared to the peaks from metal ions intercalated $Ti_3C_2T_x$. This observation indicates that water molecules are more organized (ordered) in metal ions intercalated $Ti_3C_2T_x$. The width of the peak decreases with an increase in the size of the metal ions; this means that water becomes highly ordered in K^+-intercalated $Ti_3C_2T_x$, which is consistent with narrow peaks observed from the XRD measurement [17]. We also observed the effect of the size of the metal ions on the GVDS spectra of bulk water solutions (Figs. S1 and S2 of the supplemental material) [41], showing a similar impact on the librational band in the GVDS spectra. A hump in the energy range of 140–160 meV is visible due to the two-phonon neutron scattering involving the librational band.

Stretching intramolecular O-H modes of water are present in all the $Ti_3C_2T_x$ samples [Fig. 2(d)]. It is evident from the figure that water in $Ti_3C_2T_x$ is of bulk type, giving a broad peak around $\sim$410 meV (similar to that in ice-Ih) [35]. The peaks become sharper and shift noticeably to the right after intercalation. This is attributed to the weakening of the hydrogen bond by metal ions, consequently strengthening the intramolecular covalent O-H bond. There is also a clear difference in the GVDS spectra of pristine and metal ions intercalated $Ti_3C_2T_x$ in this energy range, but the difference in terms of the size of the intercalating metal ions is not significant. As in the lower energy range, the peaks are sharper as a function of increasing ion sizes, suggesting an ordering of water molecules similar to those observed in clay materials [30,32,42]. A second hump appears at the energy range of 490–540 meV due to multiphonon neutron scattering from the combination of libration and stretching modes [43].

Ordering of water molecules after metal ions intercalation as revealed in GVDS was further investigated by molecular-dynamics simulation using the ReaxFF force field. This force field has been successfully used to understand the interfacial behavior of confined water [44,45]. The snapshots taken with a single layer of water and ions (Li^+, Na^+, and K^+, respectively) intercalated in $Ti_3C_2T_x$ layers from the ReaxFF constant-volume–constant-temperature molecular-dynamics (*NVT*-MD) simulations at 300 K are presented in Fig. 3. The initial configuration of the setup was adopted from the GCMC simulations performed in Ref. [17] to facilitate comparison. The corresponding *c*-*L* parameters determined by performing the ReaxFF constant-pressure–constant-temperature (*NPT* ensemble) simulations are of 25.90 ± 0.012, 25.51 ± 0.035, and 25.56 ± 0.017 Å for Li^+, Na^+, and K^+ ions, respectively. These differences in *c*-*L* values can be explained from the location of the ions within the water layer. Li^+ ions sit almost exactly in between the MXene interlayer surface and the water layer, and they are coordinated by two hydroxyl functional groups and two water molecules, forming a tetrahedral structure. On the other hand, K^+ (and to some extent, Na^+) ions position themselves along the center of the water layer, forming an almost planar solvation structure.

The positions of the cations intercalated between the MXene layers can be correlated with the mobility of water.

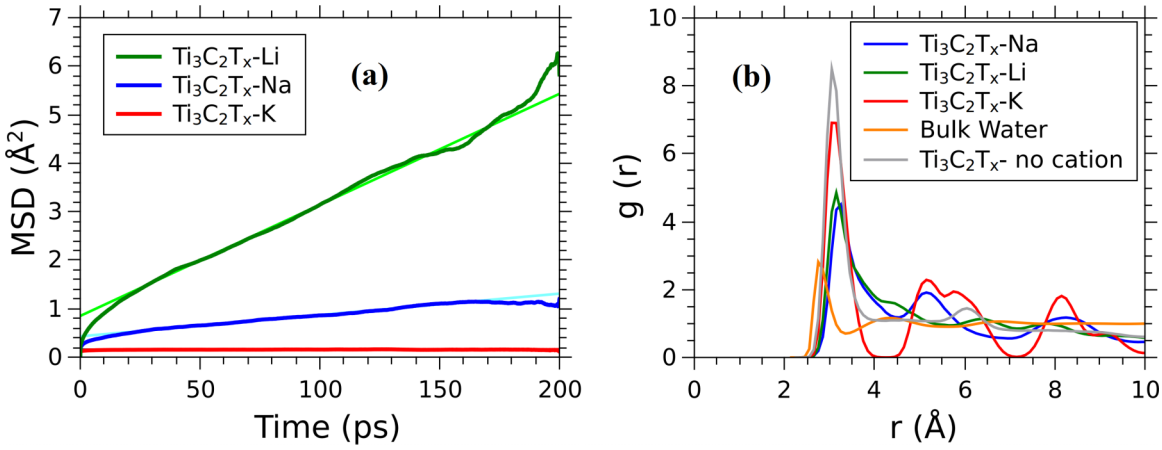

FIG. 4. Calculated (a) mean-square displacement of water molecules vs time and (b) RDF of water oxygen-oxygen ($O_w - O_w$) distances in MXene layers at 300 K in Li^+, Na^+, and K^+ ions intercalated MXenes, respectively.

The diffusion coefficient of water obtained from the calculated mean-square displacement (MSD), divided by 6 for 3D diffusion, presented in Fig. 4(a) is the highest for Li^+ ($38.53 \times 10^{-12}\,m^2\,s^{-1}$), followed by Na^+ ($7.32 \times 10^{-12}\,m^2\,s^{-1}$) and K^+ ($0.032 \times 10^{-12}\,m^2\,s^{-1}$) intercalated $Ti_3C_2T_x$. The diffusion coefficients obtained are about two orders of magnitude lower than that of bulk water ($D = 24.83 \times 10^{-10}\,m^2\,s^{-1}$) and MXene/water with no cation intercalation ($D = 11.93 \times 10^{-10}\,m^2\,s^{-1}$). The MSD-$t$ curves of bulk water and MXene/water with cation intercalation can be found in Fig. S5 of the supplemental material [41]. This trend suggests that the Li^+ ions have the least interference to the water motion as they position themselves closer to the MXene surface and away from the water layer, making the system relatively dynamic (more disordered), whereas Na^+ and K^+ ions, being more involved with the water layer, contribute to a higher resistance to the water motion (more ordering). The K^+ ions, which are the most embedded in the water, interfere most with the water. Note that the water diffusion constant for K^+-intercalated $Ti_3C_2T_x$ deviates from that reported previously in Ref. [17], as we switched off the K-K bond in the ReaxFF description—thus removing a weak, physically incorrect K^+ attractive interaction. These were obtained with a relatively high cation concentration. To evaluate potential biases related to the high cation concentration, we repeated the simulations with a three-times-lower cation concentration (22 ions/88 water), and we found that structural trends for the high-concentration results are reproduced. However, the lower concentration does not provide distinct differences in the diffusion coefficients, with the values increasing by over an order of magnitude as the ions move more freely through the water layer. The diffusion coefficients obtained are $2.97 \times 10^{-10}\,m^2\,s^{-1}$ with Li^+, $3.10 \times 10^{-10}\,m^2\,s^{-1}$ with Na^+, and $3.19 \times 10^{-10}\,m^2\,s^{-1}$ with K^+. The values appear to be within the error of each other; however, further investigation might be required. MSD-t curves for a lower concentration system can be found in Fig. S6 of the supplemental material [41].

The radial distribution function (RDF) for water, Fig. 4(b), confirms the increase in the order parameter of the water molecules from lithium to sodium to potassium, in agreement with the INS data and calculated diffusivities. The absence of a shoulder feature close to the first peak in the $Ti_3C_2T_x$-K system indicates an absence of a dynamic secondary solvation shell interchanging with the first solvation shell, which is unlike the case with Li^+ ions, where there exists a shoulder peak indicating a dynamic secondary solvation shell. Interestingly, the ordering trend for water molecules in ion-intercalated MXenes is opposite to the trend observed in bulk aqueous solutions, where the structure-making Na^+ ions suppress water diffusivity, whereas the structure-breaking K^+ ions enhance it [46]. The ordering trend for water molecules in ion-intercalated MXenes is driven essentially by the MXene morphology, which is full of different functionalities and defects [47,48].

In particular, the presence of pockets of space between the Ti-OH and the water layer is of significance, since these pockets can only be effectively occupied by the Li^+ ions, which, unlike larger cations, can reside outside the water layer. Figure 5 shows the distance of the cations and oxygen in the water layer from the oxygen in the Ti-OH group, highlighting the distinct difference in the overall position of the cations. It is found that this trend is observed also in the lower concentration system [Fig. 5(b)], and Li^+ continues to be able to access the pockets of space between Ti-OH and water. However, the lower concentration, permitting higher diffusivity, allows Li^+ to disperse into the water layer, although Na^+ and K^+ tend to retain their distinctive positions. In all cases, the results for $Ti_3C_2T_x$-Na are in between the corresponding results of K^+ and Li^+ intercalated $Ti_3C_2T_x$ systems, but closer to those of $Ti_3C_2T_x$-Li. This ordering trend, which manifests itself in the structure and diffusive and vibrational dynamics, can be related to the ion-size-dependent electrochemical performance observed from K^+, Na^+, and Li^+ intercalated $Ti_3C_2T_x$ in supercapacitor configurations [8]. Come *et al.* showed a contraction associated with Li^+ and Na^+ intercalation upon electrochemical cycling, while almost no dimensional change happened, when K^+ was electrochemically intercalated from aqueous electrolyte [49]. It has also been reported that the immersion enthalpy of $Ti_3C_2T_x$ increased from Li^+ to Na^+ and K^+ [50]. All those data show a systematic and quite substantial change in properties from lithium to potassium ion intercalation.

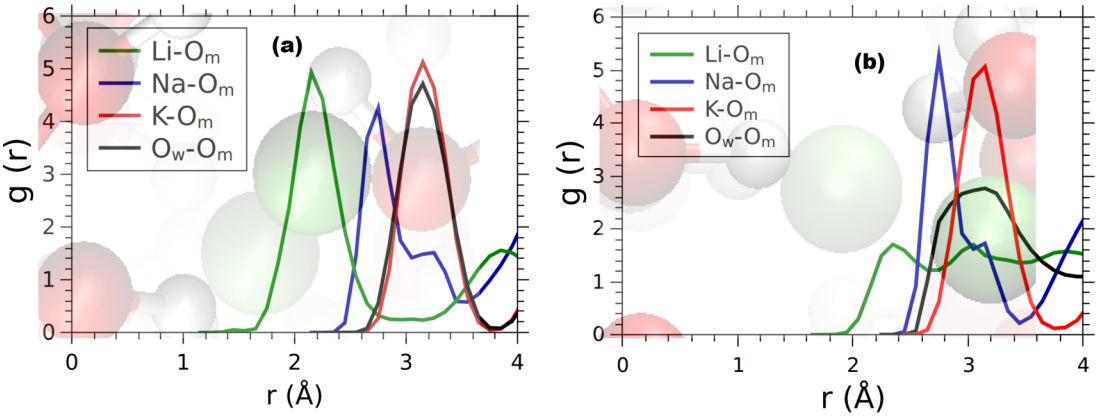

FIG. 5. RDF of MXene oxygen (O_m) and intercalated cation Li^+, Na^+, and K^+ along with oxygen in a water layer (O_w). (a) High concentration system with 72 cations/88 water, (b) low concentration system with 22 cations/88 water. Inset background: sample positions of MXene hydroxyl groups (left red/white spheres), Li cations (green spheres), and water layer (right red/white spheres).

The influence of the annealing temperature (110 and 150 °C) on the density of the vibrational states of water confined in $Ti_3C_2T_x$ is presented in Fig. S3 of the supplemental material [41]. There is a significant decrease in the intensity after 150 °C annealing because of the loss of most of the confined water. All spectra of the $Ti_3C_2T_x$ annealed at the higher temperature are very similar to that annealed at the lower temperature, except for the H_2 transitions peaks at lower energies. However, the water librational band in $Ti_3C_2T_x$ after annealing at 150 °C has a larger peak at around 120 meV, most probably due to a higher concentration of hydroxyl groups compared to H_2O water molecules in the sample (since hydroxyl groups are removed from the sample at higher temperatures than water) [11].

With an aim of exploring the impact of anions and the properties of the source of the metal ions (parent compounds) on the INS spectra of the intercalated MXenes, we explored the INS spectra collected from $Ti_3C_2T_x$ intercalated with sodium acetate ($Ti_3C_2T_x$-NaAc), and we compared them with $Ti_3C_2T_x$-Na. Those spectra are presented in Fig. S4 of the supplemental material [41]. $Ti_3C_2T_x$-NaAc contains substantially less water in contrast to $Ti_3C_2T_x$-Na. However, the spectra look almost similar in all energy ranges, suggesting that anions and the nature of the source of the metal ions do not influence the vibrational modes of the confined water. The subtle difference that could be seen might have originated from the presence of acetate groups between the MXene layers.

IV. CONCLUSION

Using inelastic neutron-scattering techniques and molecular-dynamics simulations, we have demonstrated that water in pristine $Ti_3C_2T_x$ is more bulklike in character, in comparison to water confined in nanopores of minerals, e.g., beryl, cordierite, hemimorphite [51–53], or on a nanoparticle surface of TiO_2, SnO_2, and Fe_2O_3 [21,54,55], and it shows disordered behavior. These observations are in good agreement with conclusions of an earlier QENS study of MXenes [17]. Metal ions intercalation is associated with a lower amount of water in MXene. By comparing Na^+ intercalated MXene using sodium hydroxide and sodium acetate, we found that the dynamics of water molecules remains unaffected by the source of the metal ion used to intercalate the MXene. In agreement with the MD simulations, water molecules become more ordered after metal ions intercalation, and ions strongly decrease the strength of the hydrogen bonds acting on intercalated water. Increasing the size of the metal ions enhances the ordering of water molecules. This observation provides microscopic-level rationalization of the prominent results by Lukatskaya *et al.* [8] showing the trend in specific capacitance as a function of intercalated metal ions by demonstrating a direct correlation between the cation size, the ordering of the water molecules, and the electrochemical performance. Our aim was to understand trends in the microscopic water behavior, as a function of the metal cation size, to provide guidance in tailoring MXene properties for energy and environmental applications. Thus, the findings of this research can be used to guide optimization of MXene properties by metal intercalation.

ACKNOWLEDGMENTS

This work was supported as part of the Fluid Interface Reactions, Structures and Transport (FIRST) Center, an Energy Frontier Research Center funded by the US Department of Energy, Office of Science, Office of Basic Energy Sciences. Work at ORNL's Spallation Neutron Source was sponsored by the Scientific User Facilities Division, Office of Basic Energy Sciences, US Department of Energy. Oak Ridge National Laboratory is managed by UT-Battelle, LLC, for U.S. DOE under Contract No. DEAC05-00OR22725. We would like to thank Olha Mashtalir for providing the sodium acetate intercalated MXene sample.

[1] M. Naguib, M. Kurtoglu, V. Presser, J. Lu, J. Niu, M. Heon, L. Hultman, Y. Gogotsi, and M. W. Barsoum, Adv. Mater. **23**, 4248 (2011).

[2] M. Naguib, O. Mashtalir, J. Carle, V. Presser, J. Lu, L. Hultman, Y. Gogotsi, and M. W. Barsoum, ACS Nano **6**, 1322 (2012).

[3] R. B. Rakhi, B. Ahmed, M. N. Hedhili, D. H. Anjum, and H. N. Alshareef, Chem. Mater. **27**, 5314 (2015).
[4] D. D. Sun, M. S. Wang, Z. Y. Li, G. X. Fan, L. Z. Fan, and A. G. Zhou, Electrochem. Commun. **47**, 80 (2014).
[5] Y. Xie, Y. Dall'Agnese, M. Naguib, Y. Gogotsi, M. W. Barsoum, H. L. Zhuang, and P. R. C. Kent, ACS Nano **8**, 9606 (2014).
[6] B. Anasori, M. Lukatskaya, and Y. Gogotsi, Nat. Rev. Mater. **2**, 16098 (2017).
[7] M. Naguib, V. N. Mochalin, M. W. Barsoum, and Y. Gogotsi, Adv. Mater. **26**, 992 (2014).
[8] M. R. Lukatskaya, O. Mashtalir, C. E. Ren, Y. Dall'Agnese, P. Rozier, P. L. Taberna, M. Naguib, P. Simon, M. W. Barsoum, and Y. Gogotsi, Science **341**, 1502 (2013).
[9] M. Khazaei, M. Arai, T. Sasaki, A. Ranjbar, Y. Y. Liang, and S. Yunoki, Phys. Rev. B **92**, 075411 (2015).
[10] O. Mashtalir, M. Naguib, V. N. Mochalin, Y. Dall'Agnese, M. Heon, M. W. Barsoum, and Y. Gogotsi, Nat. Commun. **4**, 1716 (2013).
[11] O. Mashtalir, M. R. Lukatskaya, A. I. Kolesnikov, E. Raymundo-Pinero, M. Naguib, M. W. Barsoum, and Y. Gogotsi, Nanoscale **8**, 9128 (2016).
[12] C. Eames and M. S. Islam, J. Am. Chem. Soc. **136**, 16270 (2014).
[13] R. R. Dessai, V. K. Sharma, S. A. Prabhudesai, S. Mitra, J. A. E. Desa, and R. Mukhopadhyay, J. Phys. Soc. Jpn. **82**, SA008 (2013).
[14] S. O. Diallo, E. Mamontov, W. Nobuo, S. Inagaki, and Y. Fukushima, Phys. Rev. E **86**, 021506 (2012).
[15] A. I. Kolesnikov, J. M. Zanotti, C. K. Loong, P. Thiyagarajan, A. P. Moravsky, R. O. Loutfy, and C. J. Burnham, Phys. Rev. Lett. **93**, 035503 (2004).
[16] M. Ghidiu, J. Halim, S. Kota, D. Bish, Y. Gogotsi, and M. W. Barsourm, Chem. Mater. **28**, 3507 (2016).
[17] N. C. Osti, M. Naguib, A. Ostadhossein, Y. Xie, P. R. C. Kent, B. Dyatkin, G. Rother, W. T. Heller, A. C. T. van Duin, Y. Gogotsi, and E. Mamontov, ACS Appl. Mater. Interf. **8**, 8859 (2016).
[18] L. Smrcok, D. Tunega, A. J. Ramirez-Cuesta, A. Ivanov, and J. Valuchova, Clays Clay Miner. **58**, 52 (2010).
[19] L. Senadheera, E. M. Carl, T. M. Ivancic, M. S. Conradi, R. C. Bowman, S. J. Hwang, and T. J. Udovic, J. Alloys Compd. **463**, 1 (2008).
[20] T. J. Udovic, W. Zhou, H. Wu, C. M. Brown, J. J. Rush, T. Yildirim, E. Mamontov, and O. Isnard, J. Alloys Compd. **446–447**, 504 (2007).
[21] E. C. Spencer, A. A. Levchenko, N. L. Ross, A. I. Kolesnikov, J. Boerio-Goates, B. F. Woodfield, A. Navrotsky, and G. S. Li, J. Phys. Chem. A **113**, 2796 (2009).
[22] Y. Xie, M. Naguib, V. N. Mochalin, M. W. Barsoum, Y. Gogotsi, X. Yu, K.-W. Nam, X.-Q. Yang, A. I. Kolesnikov, and P. R. C. Kent, J. Am. Chem. Soc. **136**, 6385 (2014).
[23] T. Hu, M. M. Hu, Z. J. Li, H. Zhang, C. Zhang, J. M. Wang, and X. H. Wang, J. Phys. Chem. A **119**, 12977 (2015).
[24] G. E. Granroth, A. I. Kolesnikov, T. E. Sherline, J. P. Clancy, K. A. Ross, J. P. C. Ruff, B. D. Gaulin, and S. E. Nagler, J. Phys.: Conf. Ser. **251**, 012058 (2010).
[25] M. B. Stone, J. L. Niedziela, D. L. Abernathy, L. DeBeer-Schmitt, G. Ehlers, O. Garlea, G. E. Granroth, M. Graves-Brook, A. I. Kolesnikov, A. Podlesnyak, and B. Winn, Rev. Sci. Instrum. **85**, 045113 (2014).
[26] P. A. Seeger, L. L. Daemen, and J. Z. Larese, Nucl. Instrum. Methods Phys. Res., Sect. A **604**, 719 (2009).
[27] T. P. Senftle, S. Hong, M. M. Islam, S. B. Kylasa, Y. Zheng, Y. K. Shin, C. Junkermeier, R. Engel-Herbert, M. J. Janik, H. M. Aktulga, T. Verstraelen, A. Grama, and A. C. T. van Duin, Comput. Mater. **2**, 15011 (2016).
[28] A. C. T. van Duin, S. Dasgupta, F. Lorant, and W. A. Goddard, J. Phys. Chem. A **105**, 9396 (2001).
[29] N. C. Osti, A. Coté, E. Mamontov, A. Ramirez-Cuesta, D. J. Wesolowski, and S. O. Diallo, Chem. Phys. **465-466**, 1 (2016).
[30] R. T. Cygan, L. L. Daemen, A. G. Ilgen, J. L. Krumhansl, and T. M. Nenoff, J. Phys. Chem. C **119**, 28005 (2015).
[31] I. Natkaniec, E. F. Sheka, K. Druzbicki, K. Holderna-Natkaniec, S. P. Gubin, E. Y. Buslaeva, and S. V. Tkachev, J. Phys. Chem. C **119**, 18650 (2015).
[32] C. M. B. Line and G. J. Kearley, J. Chem. Phys. **112**, 9058 (2000).
[33] N. W. Ockwig, J. A. Greathouse, J. S. Durkin, R. T. Cygan, L. L. Daemen, and T. M. Nenoff, J. Am. Chem. Soc. **131**, 8155 (2009).
[34] C. L. Thaper, B.A. Dasannacharya, A. Sequeira, and P. K. Iyengar, Solid State Commun. **8**, 497 (1970).
[35] J. C. Li and A. I. Kolesnikov, J. Mol. Liq. **100**, 1 (2002).
[36] T. Hu, J. M. Wang, H. Zhang, Z. J. Li, M. M. Hu, and X. H. Wang, Phys. Chem. Chem. Phys. **17**, 9997 (2015).
[37] V. F. Sears, Neutron News **3**, 26 (1992).
[38] N. C. Osti, M. Naguib, M. Tyagi, Y. Gogotsi, A. I. Kolesnikov, and E. Mamontov, Phys. Rev. Mater. **1**024004 (2017).
[39] T. Hama and N. Watanabe, Chem. Rev. **113**, 8783 (2013).
[40] C. M. B. Line and G. J. Kearley, Chem. Phys. **234**, 207 (1998).
[41] See Supplemental Material at http://link.aps.org/supplemental/10.1103/PhysRevMaterials.1.065406 for technical details, more INS spectra, and MD simulation curves.
[42] C. Corsaro, V. Crupi, D. Majolino, S. F. Parker, V. Venuti, and U. Wanderlingh, J. Phys. Chem. A **110**, 1190 (2006).
[43] J. C. Li, J. Chem. Phys. **105**, 6733 (1996).
[44] J. M. Rimsza and J. C. Du, J. Phys. Chem. C **121**, 11534 (2017).
[45] M. J. A. Qomi, M. Bauchy, F. J. Ulm, and R. J. M. Pellenq, J. Chem. Phys. **140**, 054515, (2014).
[46] P. Ben Ishai, E. Mamontov, J. D. Nickels, and A. P. Sokolov, J. Phys. Chem. B **117**, 7724 (2013).
[47] H.-W. Wang, M. Naguib, K. Page, D. J. Wesolowski, and Y. Gogotsi, Chem. Mater. **28**, 349 (2016).
[48] X. H. Sang, Y. Xie, M. W. Lin, M. Alhabeb, K. L. Van Aken, Y. Gogotsi, P. R. C. Kent, K. Xiao, and R. R. Unocic, ACS Nano **10**, 9193 (2016).
[49] J. Come, J. M. Black, M. R. Lukatskaya, M. Naguib, M. Beidaghi, A. J. Rondinone, S. V. Kalinin, D. J. Wesolowski, Y. Gogotsi, and N. Balke, Nano Energy **17**, 27 (2015).
[50] G. Sharma, E. Muthuswamy, M. Naguib, Y. Gogotsi, A. Navrotsky, and D. Wu, J. Phys. Chem. C **121**, 15145 (2017).
[51] A. I. Kolesnikov, G. F. Reiter, N. Choudhury, T. R. Prisk, E. Mamontov, A. Podlesnyak, G. Ehlers, A. G. Seel, D. J.

Wesolowski, and L. M. Anovitz, Phys. Rev. Lett. **116**, 167802 (2016).

[52] L. M. Anovitz, E. Mamontov, P. ben Ishai, and A. I. Kolesnikov, Phys. Rev. E **88**, 052306 (2013).

[53] A. I. Kolesnikov, L. M. Anovitz, E. Mamontov, A. Podlesnyak, and G. Ehlers, J. Phys. Chem. B **118**, 13414 (2014).

[54] H.-W. Wang, M. J. DelloStritto, N. Kumar, A. I. Kolesnikov, P. R. C. Kent, J. D. Kubicki, D. J. Wesolowski, and J. O. Sofo, J. Phys. Chem. C **118**, 10805 (2014).

[55] E. C. Spencer, N. L. Ross, R. E. Olsen, B. Huang, A. I. Kolesnikov, and B. F. Woodfield, J. Phys. Chem. C **119**, 9609 (2015).